Journal of **N**onlinear **A**nalysis and **O**ptimization
Vol. 16, Issue. 1, No.1 : 2025
ISSN : **1906-9685**

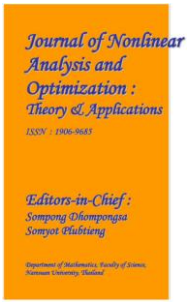

NUMERICAL ANALYSIS OF A MATHEMATICAL MODEL FOR CHEMO-IMMUNOTHERAPY IN BRAIN TUMOUR TREATMENT USING NEURAL NETWORKS

Vargees Kaviyan E Department of Mathematics, Sri Ramakrishna Mission Vidyalaya College of Arts and Science, Coimbatore-641020, India. E-mail: vargeeskaviyan@gmail.com
Jayakumar T Department of Mathematics, Sri Ramakrishna Mission Vidyalaya College of Arts and Science, Coimbatore-641020, India. E-mail: jayakumar.thippan68@gmail.com
Sujitha S Department of Science and Humanities, Sree Sakthi Engineering College, Coimbatore-641104, India. (E-mail: sujithaskr5@gmail.com)
Maheskumar D Department of Science and Humanities, Sri Krishna College of Technology, Coimbatore-42, India. (E-mail: madhana2010@gmail.com)

Abstract:
This study presents a mathematical model to simulate brain tumour dynamics under chemo-immunotherapy, leveraging a deep neural network (DNN) approach alongside the classical fourth-order Runge-Kutta (RK-4) method to compare solution accuracy. Our model incorporates the interactions of glial cells, glioma cells, neurones, and CD8+ T cells, capturing the effects of combined therapeutic strategies on tumour progression. The DNN framework was meticulously designed with varying hidden layer configurations, allowing an in-depth analysis of the relationship between model depth and approximation accuracy. The neural network methodology and the RK-4 method are compared in this paper using an exact solution as the basis for comparison. The findings indicate that the proposed method offers dependability for non-linear dynamics and is comparable to traditional techniques in a general sense. Through the use of this versatile and dependable technology, specialists are able to get a deeper understanding of the complex linkages that underlie bio-mathematical systems.

Mathematics Subject Classification:
37M05, 34K42.
Keywords and phrases: Artificial Neural Network, Brain Tumour Treatment, Chemo-immunotherapy

1. Introduction

In the context of drug-induced drug creation, mathematical models provide a framework that may be used to comprehend the behaviour of cancer cells. It is possible for physicians to forecast and manage the behaviour of malignant tumours with the use of models, which serve to decrease the amount of time and money associated with medical tests. Consequently, doctors and biologists are becoming increasingly conscious of the value of computer modelling in creating healthcare knowledge and methodologies [1, 2]. It has become possible to investigate a wide range of cancer features via the use of mathematical models of tumour growth [3, 4]. The proliferation of cancers under continuous and pulsed therapy was the subject of research conducted by Borges et al. [5], who developed a model to examine the phenomenon. Tumour-immune interaction models were utilised by Nani and Freedman [6] to explore immunotherapy for tumours. The establishment of mathematical frameworks to assess radiotherapy's effectiveness in cancer treatment was pioneered by Belostotski and Freedman [7]. McMahon, [8], highlighted therapy's use. interpretations and problems in cancer treatment. The influence of radiation on the spread of tumour cells and the proliferation of normal cells has been documented in [9, 10, 11]. Brain tumours relate to cell growth, multiplication, and sometimes unregulated development. Brain tumours arise in a number of types. While some brain tumours are

benign, some are aggressive. Tumours are generally split into two groups: primary malignancies, which develop inside the brain, and secondary cancers, sometimes known as brain metastasis tumours, which typically have spread from tumours outside the brain [12]. Different therapies vary depending on the tumour's magnitude, location, and phase. The therapy used to destroy the cancer cells must spread quicker than tumour development. Surgery, chemotherapy, radiation therapy, and immunotherapy are only a few therapies that may be used to treat brain tumours [13, 14]. The treatment choice is influenced by the sort of brain tumour and the patient's health.

DNN [15] have demonstrated great promise in resolving dynamical systems owing to their power to recognise complicated, non-linear relationships among input and output variables. DNN has shown substantial effectiveness in modelling and predicting the behaviours displayed by complicated, non-linear systems. Standard numerical approaches [16] to solve complicated non-linear differential equations need large processing resources and simplification of the underlying system, which may not always be acceptable. The utilisation of DNN bears promise for improving the administration and forecasting of sophisticated non-linear dynamical systems in many sectors [17, 18, 19]. By offering the strong technique of capturing non-linear dynamics, DNN holds great opportunities for advancing our grasp of intricate systems and inventing more effective strategies for regulating and forecasting their behaviour. Biological neurones are both the functional and structural parts of the neurological system [20, 21]. Biological neurones consist of 4 basic parts: dendrites, soma (cell body), axons, and synapses. Dendrites, soma, axon, and synapses operate as receiver, communicator, processor, and linker [22, 23]. Comparing real and artificial neurones, the input, hidden, and output layers of artificial neurones work analogously to dendrites, soma, and axons, respectively, in biological neurones. Synapses in organic neurones operate like connectors or weights in artificial neurones [24, 25, 26]. In general, developing a non-linear function that accurately relates independent and de pendent variables presents a significant challenge. Although established methods for creating mathematical models exist, their predictability remains a subject of ongoing debate and scrutiny [27, 28, 29, 30]. While solving simultaneous non-linear equations is often perceived as straightforward, this process typically requires linearisation to be feasible [31, 32]. Therefore, in this study, a biologically inspired algorithm, namely the artificial neural network (ANN), is employed to establish a relationship between the independent and dependent variables. In the study conducted by K. C. Iarosz et al. [33], it was observed that healthy cells exhibit a distinctive response in relation to the presence of various tumours and the administration of chemotherapy, highlighting the interactions between these biological entities. Addition ally, S. Khajanchi et al. [34] investigated the dynamics of cancer progression alongside the role of macrophages and CD8+ T cells in this process. Their work notably emphasises that these immune components engage with the tumour without impeding the proliferation of healthy cells. Building upon these foundational studies, another investigation [35] explored both analytical and numerical solutions for modelling the interaction between glial cells, chemo-immunotherapy, and cancerous cells. Inspired by these prior insights, the present study aims to pioneer a novel computational framework that leverages neural networks to model brain tumour responses to chemo-immunotherapy. This framework is designed to enhance the mathematical modelling process by integrating neural network methodologies into the chemo-immunotherapeutic treatment model for brain tumours, as outlined in [35]. The objective is to achieve a more accurate representation of the complex biological interactions involved, thereby advancing the potential for predictive modelling in tumour responses. The work is organised as follows: The computational modelling of a brain tumour treated with chemotherapy and immunotherapy is illustrated in section 2. The structure of DNN and the recommended neural network technique are presented in section 3. In section 4, the numerical findings are described. Section 5 is kept over for its conclusion.

2. Mathematical Model

This section provides a detailed description of a dynamic model for brain tumour progression under the influence of chemo-immunotherapy:

$$\frac{dY_1(t)}{dt} = \delta_1 Y_1(t)\left(1 - \frac{Y_1(t)}{K_1}\right) - \delta_2 Y_1(t)Y_2(t) - \frac{\delta_3 Y_1(t)Y_4(t)}{\overline{m_1} + Y_1(t)}, \quad (1)$$

$$\frac{dY_2(t)}{dt} = \delta_4 Y_2(t)\left(1-\frac{Y_2(t)}{K_2}\right) - \delta_5 Y_1(t)Y_2(t) - \frac{\delta_6 Y_2(t)Y_4(t)}{Y_2(t)+\overline{m_2}} - \frac{\left(\delta_7 Y_5(t)+\delta_8 Y_6(t)\right)Y_2(t)}{Y_2(t)+\overline{m_3}}, \quad (2)$$

$$\frac{dY_3(t)}{dt} = \delta_9 \dot{Y_1}(t)R\left(-\dot{Y_1}\right)Y_3(t) - \frac{\delta_{10}Y_3(t)Y_4(t)}{Y_3(t)+\overline{m_4}}, \quad (3)$$

$$\frac{dY_4(t)}{dt} = \delta_{11} - \delta_{12}Y_4(t), \quad (4)$$

$$\frac{dY_5(t)}{dt} = \delta_{13}Y_5(t)\left(1-\frac{Y_5(t)}{K_4}\right) - \frac{\delta_{14}Y_2(t)Y_5(t)}{\overline{m_5}+Y_2(t)}, \quad (5)$$

$$\frac{dY_6(t)}{dt} = \frac{\delta_{15}Y_2(t)Y_6(t)}{\overline{m_6}+Y_2(t)} - \delta_{16}Y_6(t) - \frac{\delta_{17}Y_2(t)Y_6(t)}{\overline{m_7}+Y_2(t)} + \delta_{18}\delta_{19}. \quad (6)$$

The mathematical model under consideration consists of six distinct components, each representing a crucial biological or pharmacological factor influencing brain tumour dynamics. The model incorporates the following variables: $Y_1(t)$, denoting the concentration of glial cells in units of Kg/m^3; $Y_2(t)$, the density of glioma cells (tumour cells) also in Kg/m^3; $Y_3(t)$, the concentration of neurone cells measured in Kg/m^3; $Y_4(t)$, the concentration of the chemotherapeutic agent in mg/m^2; $Y_5(t)$, the density of macrophages in Kg/m^3; and $Y_6(t)$, the concentration of CD8+ T cells also measured in Kg/m^3. Each of these variables is governed by a system of differential equations that capture their interactions over time.

$$R(\epsilon) = \begin{cases} 0, & \epsilon < 0, \\ \frac{1}{2}, & \epsilon = 0, \\ 1, & \epsilon > 0. \end{cases} \quad (7)$$

In (1), (2), and (5), the first term represents the proliferation of cells, describing their natural growth or replication over time. In (1) and (2), the second term models the interaction between healthy cells and cancerous glioma cells. This term accounts for how the healthy glial and neurone cells are affected by the presence of tumour cells. The third term in (1) and (2) represents the effect of the chemotherapeutic agent, $Y_4(t)$, on both glial and tumour cells. This term quantifies how the administered drug alters the population dynamics of these cells. In (2), the final term accounts for the immune-mediated elimination of glioma cells $Y_2(t)$, through their interaction with macrophages ($Y_5(t)$) and CD8+ T cells ($Y_6(t)$). This term highlights the role of the immune system in targeting and reducing tumour cells. (3) focuses on neurone cells ($Y_3(t)$), where the first term represents the neurone population's dependence on glial cells ($Y_1(t)$), as glial cells play a key supportive role in neurone function. The second term captures the interaction between neurones and the chemotherapeutic agent, reflecting how the drug may impact healthy neurons. In (4), the first term describes the dynamics of the chemotherapeutic agent, $Y_4(t)$, particularly its rate of administration or concentration over time. The second term represents the natural decay or degradation of the drug in the body as the concentration diminishes due to metabolic processes and other clearance mechanisms. (5) models the behaviour of macrophages ($Y_5(t)$). The final term in this equation signifies the deactivation or reduction of macrophages due to interactions with glioma cells, $Y_2(t)$. This term reflects how tumour cells can evade or suppress immune responses by reducing macrophage activity. Finally, in (6), the first term reflects the recruitment of CD8+ T cells ($Y_6(t)$) by glioma cells ($Y_2(t)$), as tumour cells may induce an immune response by attracting T cells to the site of malignancy. The second term describes the natural decay rate of T cells, which can occur due to the brain's inflammatory response or other physiological factors. The third term represents the elimination of T cells due to their interaction with glioma cells, which may reduce the population of T cells as they engage and destroy tumour cells. Parameters δ_{18} and δ_{19} are key factors in the model, where δ_{18} measures the efficacy of the therapy and δ_{19} represents an external source of CD8+ T cells, potentially from immunotherapy treatments.

Table: 1. List of symbols and abbreviations.

Parameter	Values	Source
δ_1	0.0068 day^{-1}	Proliferation rate [36, 37]
δ_5	0.68 day^{-1}	Proliferation rate [36, 37]
δ_9	0-0.02	Loss influences [36]
δ_3, δ_{10}	$2.4 \times 10^{-5}\ m^2(day.mg)^{-1}$	Predation Coefficients [36 38]
δ_6	$0.24 \times 10^{-3}\ m^2(day.mg)^{-1}$	Predation Coefficients [36, 38]
δ_{11}	0-400 $mg(m^2.day)^{-1}$	Chemotherapy rate [39]
δ_{12}	$0.2day^{-1}$	Chemotherapy rate [40]
$\overline{m_1}, \overline{m_2}, \overline{m_3}$	510	Holling type 2 [41]
δ_2	$3.6 \times 10^{-5} day^{-1}$	Competition Coefficients [36]
δ_5	$3.6 \times 10^{-6} day^{-1}$	Competition Coefficients [36]
$K = K_1, K_2, K_3$	510 kg/m^3	Carrying Capacity [41]

Table: 2. Values of Normalized Parameter.

Parameter	Values	Source
δ_7	0.069943	[42]
δ_8	2.74492	[42]
$\overline{m_3}$	0.90305	[43]
δ_{13}	0.3307	[42]
δ_{14}	0.0194	[42]
$\overline{m_5}$	0.030584	[43]
δ_{15}	0.1245	[44]
$\overline{m_6}$	2.8743	[44]
δ_{16}	0.0074	[42]
δ_{17}	0.01694	[43]
$\overline{m_7}$	0.378918	[43]

3. Chemo-Immunotherapy Model of Brain Tumour with Neural Network

We employed a DNN-based technique to solve a system of non-linear differential equations to emulate the before described difficulty. To solve differential equations, DNN initially codes the equation as a loss function for optimal concerns, and it then utilises it to limit the deficit through various optimising procedures. A detailed discussion of the functioning and efficiency of neural networks is given here.

3.1. Data Acquisition

To approximate the solution of a system of equations using a neural network, the type of data typically employed comprises input features and the corresponding values of the dependent variable. In the context of a differential equation system, the input features are the parameters. It is necessary to determine the values for these parameters and the time interval for estimation. The solutions of the system [1]-[6] at time t are represented as $Y_1(t)$, $Y_2(t)$, $Y_3(t)$, $Y_4(t)$, $Y_5(t)$, and $Y_6(t)$. These solutions are unknown and need to be estimated by a DNN. Utilising the data set, the fully connected layer can estimate the dependent variable for new input configurations by identifying underlying patterns and relationships between the dependent variable values and the input properties. The NeuroDiffEq Python package is configured to divide the data set into training and testing sets, facilitating this estimation process.

3.2. Design of a Neural Network

As outlined by the proposed technique, a fully connected neural network (FCNN) serves as the fundamental framework to achieve the research objectives. The specified model is structured such that

each neural network, tailored for the dependent variables, comprises one input layer, five fully connected hidden layers, and one output layer. Each of the hidden layers contains 32 neurons. An activation function excites the input at each stage before passing it to the subsequent layer, with the primary role of introducing non-linearity to the network and thereby facilitating neuronal activation. The Tanh activation function, noted for its continuous and smooth properties, is employed in our design. This characteristic of the Tanh activation function is particularly beneficial for gradient-based optimisation strategies, such as back propagation, due
to the network's continuous and differentiable outputs.

To optimise the neural network, we manually adjusted various parameters in the DNN baseline design, including the learning rate, activation function, optimisation method, number of layers, and number of neurones per layer. The internal workings of the neural network are depicted in Figure [1], which illustrates the simulation of a particular scenario. The network comprises several layers interconnected by weighted connections: input, hidden, and output layers. Each layer performs specific computations to evaluate the system's performance.

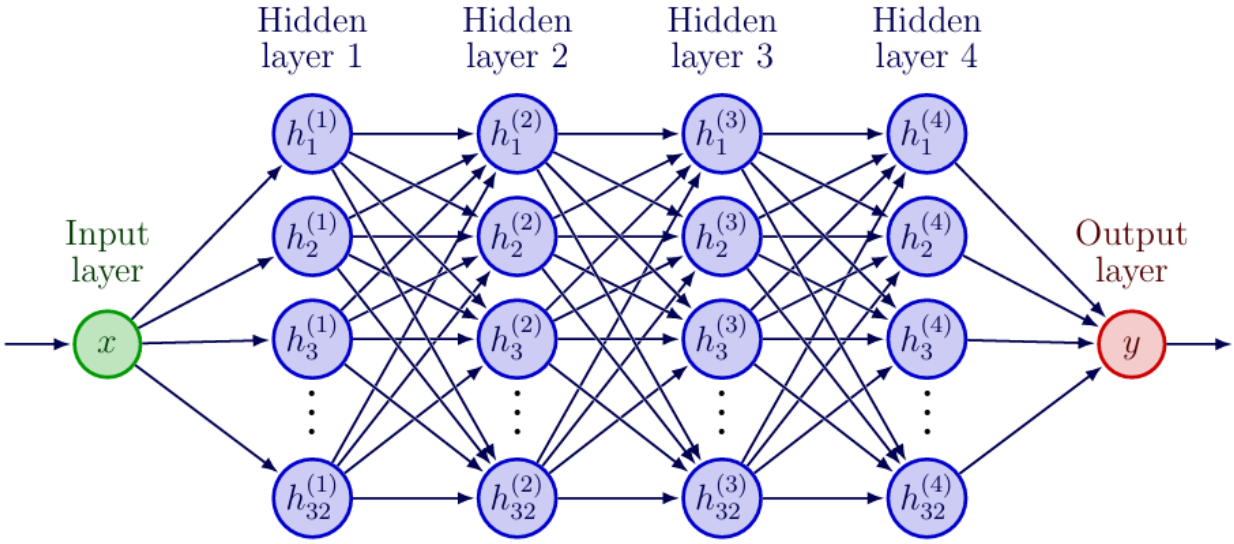

Figure 1: Design of Neural Network.

3.3. Training and Loss Validation of the Model

The initial configuration is completed, followed by the stochastic initialisation of weights and biases to commence model training. We set a learning rate of 0.01 and trained over 3000 epochs. The input data is propagated through the network, with the output transmitted to subsequent layers after applying the activation function and calculating the average weighted inputs for each layer. The activation function evaluates whether a neurone should activate to relay the output to the next layer based on a predetermined threshold. This process iterates until reaching the output layer, enhancing the expressive capability of the fully connected layer through the activation function.

The model's performance is evaluated using the predicted output, calculated via an appropriate loss function. Mean squared error (MSE) is employed to quantify the average disparity between the predicted and actual output values, thus assessing the model's efficacy during training.

$$MSE = \frac{1}{n}\left[\sum_{i=1}^{n}(p_i - q_i)\right], \qquad (8)$$

where, n = the total number of data points in the dataset,
p_i= the true value of the j-th sample,
q_j represents the predicted value for the same sample.

The model's objective is to improve prediction accuracy by minimising the loss function through optimisation techniques during the back propagation process, as described in . For this purpose, we employed the Adam (Adaptive Moment Estimation) algorithm, an optimisation method that leverages both energy-based momentum and an adaptive learning rate and integrates these components for more efficient parameter updates.

The Adam algorithm can be expressed analytically by considering the following:

$$\begin{cases} q_t & = \lambda q_{t-1} + (1-\lambda) w_t^2, \\ u_t & = \sqrt{\alpha u_{t-1} + (1-\alpha) w_t^2}, \\ v_{t+1} & = q_t - \beta \dfrac{(1-\alpha) q_t}{(1-\lambda) u_{t+\gamma}}. \end{cases}$$

At each iteration t, the first-moment estimate, denoted by q_t, corresponds to the mean of the gradients evaluated at time t. The parameters λ and α introduce exponential decay factors that govern the influence of past gradients in the update process. Concurrently, the variance of the gradients at each time step is captured by u_t, which represents the second-moment estimate. The gradient itself, computed at time t, is symbolised by w_t.

The learning rate, β, controls the magnitude of the parameter update at each step, influencing the rate at which the model converges to an optimal solution. The updated parameter value at time $t+1$, denoted as v_{t+1}, reflects the cumulative impact of the gradients up to the current iteration, incorporating both the first- and second-moment estimates.

Through the combination of these factors, Adam dynamically adjusts the learning rate for each parameter, ensuring that convergence is both efficient and stable, especially in scenarios involving noisy gradients or sparse data. This makes Adam particularly effective for deep learning applications, where large datasets and complex architectures demand robust optimisation techniques.

3.4. Assessment of the Effectiveness of the Model

Upon completing the framework's training, we proceed to the validation phase. This phase is crucial for optimising the model's performance, achieved by adjusting parameters such as the learning rate and the number of epochs. Ultimately, the results are compared with those obtained using a traditional numerical method to evaluate the accuracy and loss of the proposed methodology. The Python programming language is employed to simulate and visualise the outcomes of our differential equation system model.

4. Numerical Simulations

This section will present the simulation results obtained using the proposed DNN approach. For the brain tumour model described by equations [1] to [6], we apply the suggested FCNN methodology, accompanied by detailed explanations of each step in the simulation process. Tables 1 and 2 list and analyse the values of key parameters within the brain tumour model, providing insight into their roles in simulating tumour dynamics. To assess the performance of the FCNN model, we compare it with the classical fourth-order RK-4 method, employing the RK-4 method as a reference for the exact solution. For validation, the FCNN was trained on the defined brain tumour model along with the specified initial conditions to evaluate the neural network's accuracy. Differences between the FCNN-generated results and the exact solutions are used as a measure of accuracy in these simulations. The entire simulation process, including the training and validation of the neural network model, was implemented using Python.

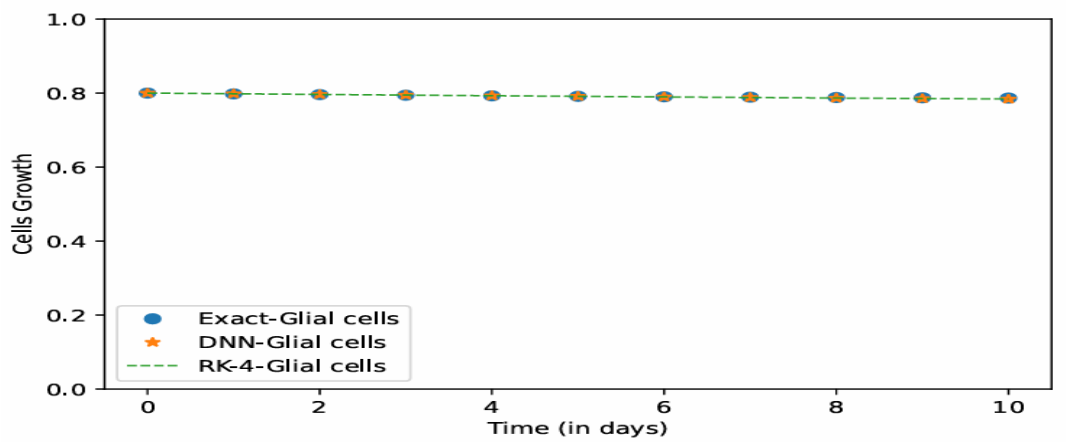

Figure 2. Comparing the Exact solution of glial cells with DNN and RK-4

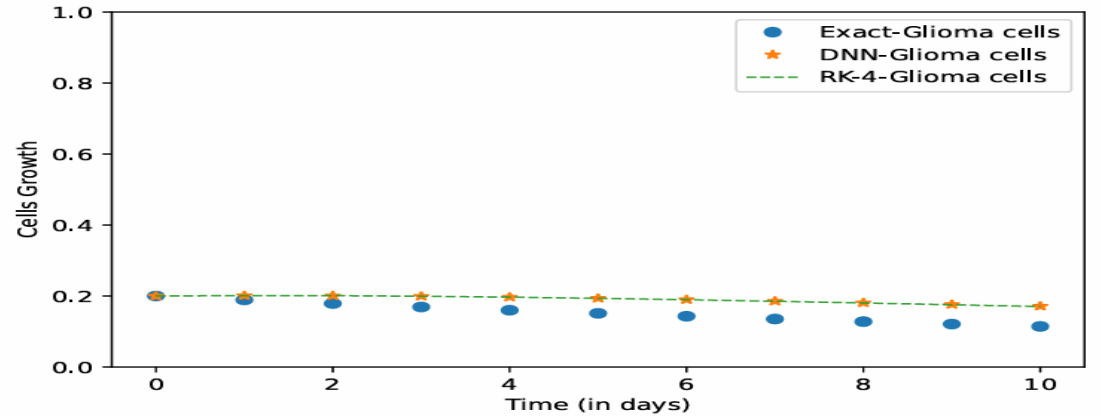

Figure 3. Comparing the Exact solution of glioma cells with DNN and RK-4.

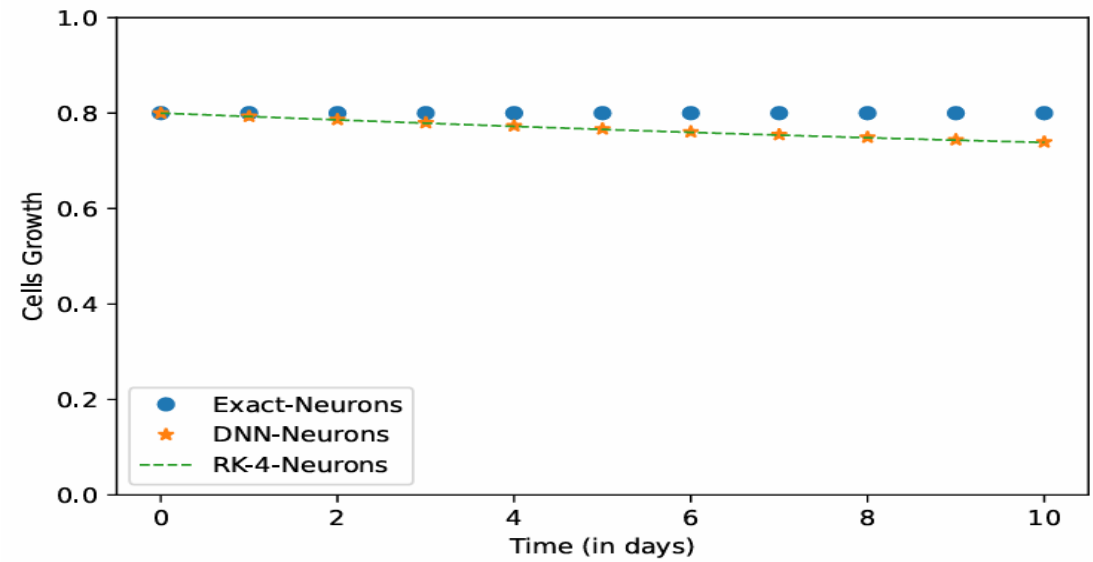

Figure 4. Comparing the Exact solution of Neurons with DNN and RK-4.

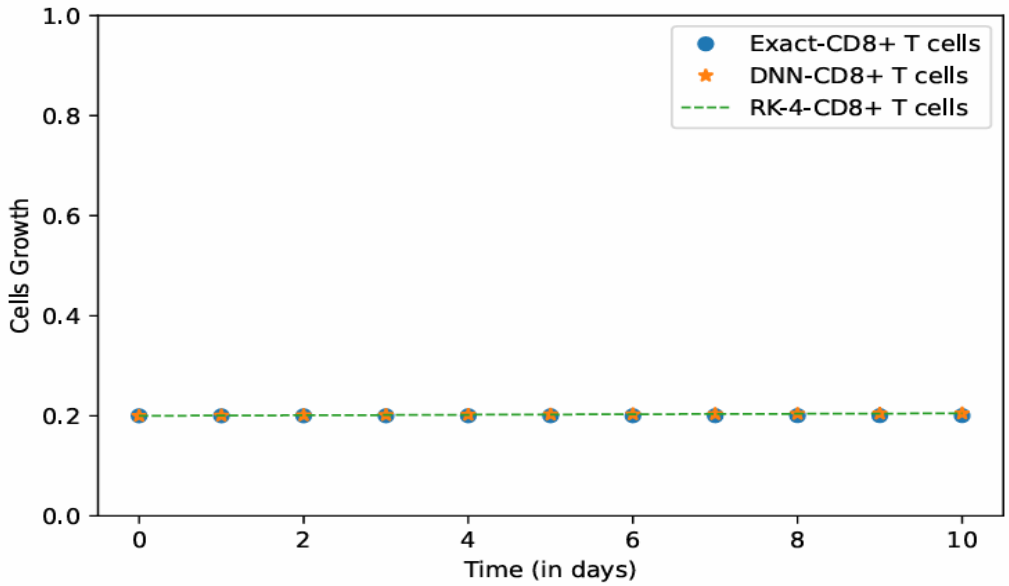

Figure 5. Comparing the Exact solution of CD8+ T cells with DNN and RK-4.

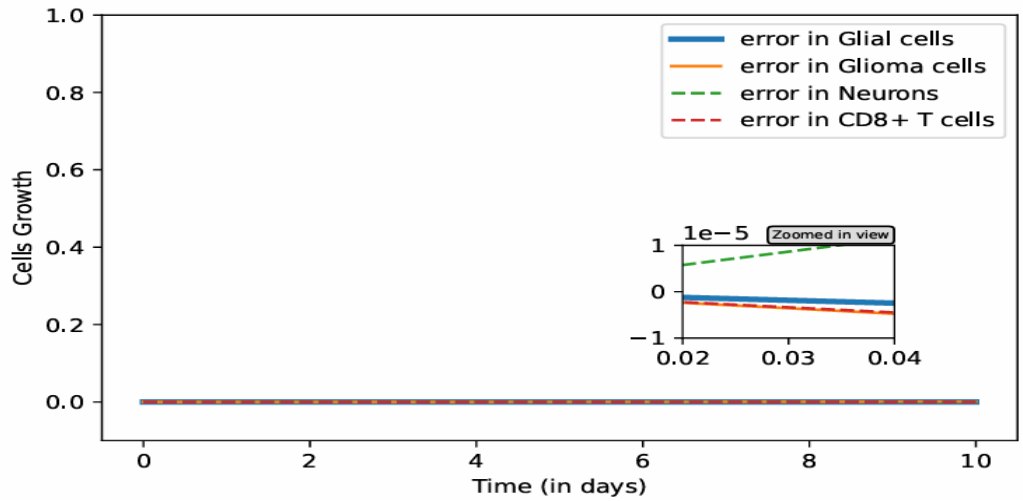

Figure 6. Error of ANN solution from numerical solutions

Figures 2 to 5 offer a comparative analysis between the exact solution, the fourth-order RK-4 method, and the solutions derived from the DNN model. These graphical representations reveal how accurately the DNN approximates the solution for the non-linear dynamical system governing brain tumour behaviour. Specifically, in Figures 2 to 5, the plots showcase star lines indicating the DNN approximation, dashed lines for the RK-4 method, and dotted lines representing the exact solution, all of which align closely, highlighting the predictive accuracy of the DNN approach.

Although traditional numerical techniques like the RK-4 method are reliable, they can become computationally intensive, especially when applied to complex systems or models of high dimensionality. As the number of iterations increases, the computational cost rises significantly. By contrast, once trained, the DNN model offers a substantial advantage by delivering predictions and solutions much faster than iterative numerical methods, making it highly suitable for applications requiring rapid computations.

Figure 6 illustrates the error between an ANN solution and a numerical reference solution over a 10-day period, specifically for modelling the growth dynamics of various cell types involved in brain tumour responses. The x-axis represents time in days, while the y-axis shows the cell growth error. The legend indicates four cell types: glial cells (blue), glioma cells (yellow), neurones (green), and CD8+ T cells (red). Remarkably, each error line is almost flat at zero, suggesting that the ANN solution

closely approximates the numerical solution with minimal deviation across all cell types throughout the time frame. This near-zero error indicates a highly accurate ANN model, likely due to an effective selection of network architecture—such as the appropriate number of hidden layers and neurones—and a well-curated training dataset. Such precision implies that the ANN can reliably simulate cell growth without significant computational cost, providing a valuable approximation method for understanding cell dynamics in complex treatments like chemo-immunotherapy. This high accuracy positions the ANN as a practical tool for predicting cell behaviour in brain tumour models, potentially aiding treatment simulations where computational efficiency and accuracy are crucial.

Table 3. Error analysis of exact solution of glial cells, with ANN and RK-4.

TIME	EXACT	ANN	RK	ANN Error	RK-4 Error
0.0	0.8000000000	0.8000000000	0.8000000000	0.0000000000	0.0000000000
1.0	0.7978668340	0.7981420681	0.7982038702	0.0002752340	0.0003370362
2.0	0.7959366469	0.7963166615	0.7964140977	0.0003800145	0.0004774507
3.0	0.7941979384	0.7945537524	0.7946502020	0.0003558139	0.0004522636
4.0	0.7926398144	0.7928444033	0.7929282796	0.0002045889	0.0002884652
5.0	0.7912519579	0.7911878840	0.7912610203	0.0000640739	0.0000090624
6.0	0.7900246016	0.7895942480	0.7896579860	0.0004303536	0.0003666156
7.0	0.7889485002	0.7880719710	0.7881260357	0.0008765293	0.0008224645
8.0	0.7880149048	0.7866241655	0.7866698020	0.0013907393	0.0013451028
9.0	0.7872155372	0.7852515923	0.7852921478	0.0019639449	0.0019233894
10.0	0.7865425663	0.7839548428	0.7839945698	0.0025877236	0.0025479965

Table 4. Error analysis of exact solution of glioma cells, with ANN and RK-4.

TIME	EXACT	ANN	RK	ANN Error	RK-4 Error
0.0	0.2000000000	0.2000000000	0.2000000000	0.0000000000	0.0000000000
1.0	0.1891285924	0.2010853557	0.2012045324	0.0119567634	0.0120759400
2.0	0.1788481222	0.2008208816	0.2009446381	0.0219727594	0.0220965159
3.0	0.1691264680	0.1993910693	0.1994299778	0.0302646013	0.0303035098
4.0	0.1599332541	0.1969308809	0.1968850920	0.0369976268	0.0369518379
5.0	0.1512397561	0.1936663336	0.1935275380	0.0424265775	0.0422877818
6.0	0.1430188109	0.1895531699	0.1895531699	0.0467950983	0.0465343590
7.0	0.1352447320	0.1851288318	0.1851288318	0.0502900206	0.0498840998
8.0	0.1278932289	0.1809636917	0.1803908653	0.0530704628	0.0524976364
9.0	0.1209413318	0.1762245754	0.1754472670	0.0552832436	0.0545059353
10.0	0.1143673192	0.1714313668	0.1703816222	0.0570640476	0.0560143031

Table 5. Error analysis of exact solution of Neurons, with ANN and RK-4.

TIME	EXACT	ANN	RK	ANN Error	RK-4 Error
0.0	0.8000000000	0.8000000000	0.8000000000	0.0000000000	0.0000000000
1.0	0.7999905907	0.7931347859	0.7928471594	0.0068558048	0.0071434313
2.0	0.7999811815	0.7864673308	0.7857823996	0.0135138507	0.0141987819
3.0	0.7999717724	0.7798260126	0.7788806642	0.0201457599	0.0210911082
4.0	0.7999623634	0.7732104191	0.7722010199	0.0267519443	0.0277613435
5.0	0.7999529546	0.7668202288	0.7657874654	0.0331327258	0.0341654892
6.0	0.7999435458	0.7606870790	0.7596707044	0.0392564668	0.0402728414
7.0	0.7999341372	0.7548393072	0.7538703788	0.0450948300	0.0460637584
8.0	0.7999247287	0.7493191969	0.7483973569	0.0506055318	0.0515273718
9.0	0.7999153202	0.7441593856	0.7432558204	0.0557559347	0.0566594998
10.0	0.7999059119	0.7393743307	0.7384450299	0.0605315812	0.0614608821

Table 6. Error analysis of exact solution of CD8+ T cells, with ANN and RK-4.

TIME	EXACT	ANN	RK	ANN Error	RK-4 Error
0.0	0.2000000000	0.2000000000	0.2000000000	0.0000000000	0.0000000000
1.0	0.2000324617	0.2004285480	0.2005407762	0.0003960863	0.0005083145
2.0	0.2000677936	0.2010049192	0.2010804895	0.0009371256	0.0010126959
3.0	0.2001058055	0.2015871710	0.2016140294	0.0014813656	0.0015082240
4.0	0.2001463177	0.2021273721	0.2021371244	0.0019810544	0.0019908067
5.0	0.2001891607	0.2026134455	0.2026463832	0.0024242848	0.0024572225
6.0	0.2002341745	0.2030818691	0.2031392516	0.0028476946	0.0029050772
7.0	0.2002812077	0.2035494133	0.2036139153	0.0032682056	0.0033327076
8.0	0.2003301178	0.2040097540	0.2040691799	0.0036796362	0.0037390622
9.0	0.2003807699	0.2044463071	0.2045043505	0.0040655372	0.0041235806
10.0	0.2004330371	0.2048418750	0.2049191217	0.0044088380	0.0044860847

Tables 3, 4, 5, and 6 provide a detailed numerical analysis of the performance of the DNN in relation to both the analytical solution and the RK-4 method, allowing for a thorough examination of each approach's accuracy.

The MSE between the analytical solution and the DNN results for glial cells, glioma cells, neurones, and CD8+ T cells are, respectively, $1.257617015654127 \times 10^{-6}$, $1.6871304788930305 \times 10^{-3}$,

$1.3961138369358035 \times 10^{-3}$, and $7.393451449566494 \times 10^{-6}$. In comparison, the MSE values between the analytical solution and the RK-4 method for the same cellular components are $1.222677328 \times 10^{-6}$, $1.656768436768 \times 10^{-3}$, $1.456547481051 \times 10^{-3}$, and $7.655982046 \times 10^{-6}$. This comparative analysis shows that both DNN and RK-4 methods yield results in close approximation to the analytical solution, suggesting that each method possesses a comparable degree of accuracy. Further, examining the DNN performance across varying hidden layer configurations reveals the impact of network depth on approximation accuracy. With 3 hidden layers, the DNN yields MSE values of $9.262903642 \times 10^{-6}$, $1.674901728324 \times 10^{-3}$, $1.454271966192 \times 10^{-3}$, and $8.034574139 \times 10^{-6}$. Increasing to 5 hidden layers, the MSE values improve to $1.089336208 \times 10^{-6}$, $1.679083839423 \times 10^{-3}$, $1.41948378053 \times 10^{-3}$, and $7.034810301 \times 10^{-6}$, respectively. This comparison highlights that increasing the number of hidden layers in the DNN tends to enhance the model's approximate accuracy, potentially allowing it to surpass the RK-4 method in certain scenarios. Conversely, increasing the order of the RK method may also contribute to improved approximation, occasionally exceeding the performance of the DNN. Hence, the selection between these methods may depend on the specific requirements of accuracy and computational complexity within a given application.

5. Discussion and Conclusions

The presented study investigates the mathematical modelling of brain tumour dynamics under the influence of chemo-immunotherapy, comparing the accuracy of solutions obtained through a DNN approach and the classical RK-4 method. Through numerical simulations, the study assesses the precision of DNN-based solutions relative to RK-4 and analytical solutions across different cell populations, including glial cells, glioma cells, neurones, and CD8+ T cells.

Our findings indicate that both the DNN and RK-4 methods provide results closely aligned with the analytical solution, validating their effectiveness in modelling the complex behaviours of brain tumours. The MSE values demonstrate that the DNN approach, when structured with sufficient hidden layers, can approximate the analytical solution with comparable accuracy to the RK-4 method. Specifically, increasing the hidden layers within the DNN results in a decrease in error, suggesting that the model's depth enhances its capacity to capture nuanced relationships in the data generated from the chemo-immunotherapy model. For instance, while the DNN with 3 hidden layers achieves a reasonable approximation, the configuration with 5 hidden layers achieves even lower MSE values, underscoring the importance of network depth in enhancing model fidelity.

However, the results also reveal that increasing the order of the RK method could yield improved approximations as well, demonstrating that, with appropriate tuning, RK methods remain a competitive approach for this type of modelling. The relative performance of DNN and RK-4 varies across the cellular populations studied, indicating that certain configurations may be better suited to specific cell types within the tumour micro-environment.

In conclusion, this research highlights the potential for DNNs to approximate complex biological models with high accuracy, particularly when optimized with an appropriate network structure. Moreover, while DNNs show promise in potentially outperforming RK methods in specific instances, the RK-4 method remains robust, especially with an increase in order. Thus, the choice between DNN and RK-4 methods should be made based on the specific accuracy requirements, computational resources, and characteristics of the cell populations modelled. Future work may explore further tuning DNN architectures or hybrid approaches that integrate traditional numerical methods and neural networks to achieve even more accurate and computationally efficient solutions for modelling chemo-immunotherapy dynamics in brain tumours.

Declarations

Funding

Not applicable.

Code availability

Not applicable.

Conflict of interest

There is no conflict of interest declared by the authors.

Author Contribution

Each contributor made an equal contribution to the paper. The article was reviewed and approved by all writers.

References

[1] Swan GW, Role of optimal control theory in cancer chemotherapy, Mathematical Biosciences, 101(2)(1990),237–284, doi:10.1016/0025-5564(90)90021-P.

[2] S Pinho, H Freedman and F Nani, A Chemotherapy model for the treatment of cancer with metastasis, Mathematical and Computer Modelling, 36(7-8)(2002), 773–803, doi:10.1016/S0895-7177(02)00227-3.

[3] S.T.R. Pinho, F.S. Barcelar, R.F.S. Andrade, H.I. Freedman, A mathematical model for the effect of anti-angiogenic therapy in the treatment of cancer tumors by chemotherapy, Nonlinear Analysis Real World Applications, 14(1)(2013), 815–828, doi:10.1016/j.nonrwa.2012.07.034.

[4] J.S. Spratt, T.L. Spratt, Rates of growth of pulmonary metastases and host survival, Annals of Surgery, 159(2)(1964), 161–171, doi:10.1097/00000658-196402000-00001.

[5] F.S. Borges, K.C. Iarosz, H.P. Ren, A.M. Batista, M.S. Baptista, R.L. Viana, S.R. Lopes, C. Grebogi, Model for tumour growth with treatment by continuous and pulsed chemotherapy, BioSystems, 116(2014), 43-48, doi:10.1016/j.biosystems.2013.12.001.16

[6] F. Nani, H.I. Freedman, A mathematical model of cancer treatment by immunotherapy, Mathematical Biosciences , 163(2)(2000), 159-199, doi:10.1016/S00255564(99)00058-9.

[7] G. Belostotski, H. Freedman, A control theory model for cancer treatment by radiotherapy, International Journal of Pure and Applied Mathematics, 25(4)(2005), 447480.

[8] S.J. McMahon, The linear quadratic model: usage, interpretation and challenges, Physics in Medicine and Biology, 64(1)(2018), 01TR01, doi:10.1088/13616560/aaf26a.

[9] B. Emami, Tolerance of Normal Tissue to Therapeutic Radiation, Reports of Radiotherapy and Oncology, 1(1)(2013), 123-127.

[10] M.H. Nasir, F.M. Siam, Simulation and sensitivity analysis on the parameter of non-argeted irradiation effects model, Journal of technology, 81(1)(2019), 133-142,doi:10.11113/jt.v81.12448.

[11] H. Rashid, F. Mohd Siam, N. Maan, Parameter Estimation for a Model of Ionizing Radiation Effects on Targeted Cells using Genetic Algorithm and Pattern Search Method, Mathematika, 34(2018), 1-13, doi:10.11113/MATEMATIKA.V34.N3.1134.

[12] J.Peiffer, P.Kleihues and H.J Scherer., Pioneer in glioma research, Brain Pathology, 9(2)(1999), 241- 245, doi:10.1111/j.1750-3639.1999.tb00222.x.

[13] Deboroah et al., Low-Grade Gliomas, AlphaMed Press, 19(4)(2014), 403–413, doi:10.1634/theoncologist.2013-0345.

[14] Shibamoto Y, Sugie C, Iwata H, Radiotherapy for metastatic brain tumors, International Journal Clinical Oncology, 14(4)(2009), 281–288, doi:10.1007/s10147-0090915-2.

[15] Rahman J, Faiza M, Akhtar A, Sana D, Mathematical modeling and simulation of biophysics systems using neural network, International Journal of Modern Physics B, 38(5), (2024), 2450066, doi:10.1142/S0217979224500668.

[16] Zarnan J.A, Hameed W.M., Kanbar A.B., New Numerical Approach for Solution of Nonlinear Differential Equations, Journal of Hunan University Natural Sciences, 49(7)(2022), 163–170, doi:10.55463/issn.1674-2974.49.7.18.

[17] Li Y, Wei H, Han Z, Huang J, Wang W, Deep learning-based safety helmet detection in engineering management based on convolutional neural networks, Advances in Civil Engineering, 2020(1)(2020), 9703560, doi:10.1155/2020/9703560. 17

[18] Sahu A, Rana K.P.S, Kumar V, An application of deep dual convolutional neural net-work for enhanced medical image denoising, Medical & Biological Engineering & Computing, 61(5)(2023), 991– 1004, doi:10.1007/s11517-022-02731-9.

[19] Pan G, Zhang P, Chen A, Deng Y, Zhang Z, Lu H, Zhu A, Zhou C, Wu Y, Li S, Aerobic glycolysis in colon cancer is repressed by naringin via the HIF1A pathway, Journal of Zhejiang University-SCIENCE B, 24(2023), 221–231, doi:10.1631/jzus.B2200221.
[20] Yuste R, Denk W, Dendritic spines as basic functional units of neuronal integration. Nature, 375(6533)(1995), 682–684, doi:10.1038/375682a0.
[21] Zhang L, Artificial neural network model design and topology analysis for FPGA implementation of Lorenz chaotic generator. In 2017 IEEE 30th Canadian conference on electrical and computer engineering (CCECE), (2017) 1–4, doi:10.1109/CCECE.2017.7946635. [22] Anderson J A, A simple neural network generating an interactive memory, Mathematical Bioscience, 14(3–4)(1972), 197–220, doi:10.1016/0025-5564(72)90075-2.
[23] Guzma´ n-Ramı´ rez E, Garcia I, Garcı´ a-Jua´ rez M, A "learning by design" application for modeling, implementing, and evaluating hardware architectures for artificial neural networks at undergraduate level, Computer Application in Engineering Education, 27(5)(2019), 1236–1252, doi:10.1002/cae.22148.
[24] Adel A, Salah K, Model order reduction using artificial neural networks. In 2016 IEEE International Conference on Electronics, Circuits and Systems (ICECS), (2016), 89–92, doi:10.1109/ICECS.2016.7841139.
[25] Grillo SA A linear relation between input and first layer in neural networks, Annals of Mathematics and Artificial Intelligence, 87(4)(2019), 361–372, doi:10.1007/s10472019-09657-3.
[26] Venkadesan A, Harmonic current estimation of a nonlinear load using artificial neural network, Intelligent paradigms for smart grid and renewable energy systems, (2021), 337–359, doi:10.1007/978-981-15-9968-2 11.
[27] Ahmad F, Isa NAM, Hussain Z, Osman MK, Sulaiman SN, A GA-based feature selection and parameter optimization of an ANN in diagnosing breast cancer, Pattern Analysis and Application, 18(4)(2015), 861–870, doi:10.1007/s10044-014-0375-9.
[28] Ghiassi M, Saidane H, A dynamic architecture for artificial neural networks, Neurocomputing, 63(2005), 397–413, doi:10.1016/j.neucom.2004.03.014.18
[29] Heinze-Deml C, Peters J, Meinshausen N, Invariant causal prediction for nonlinear models, Journal of Causal Inference, 6(2)(2018), 20170016, doi:10.1515/jci-20170016.
[30] Vaidyanathan S, Pehlivan I, Dolvis LG, Jacques K, Alcin M, Tuna M, Koyuncu I, A novel ANN-based four-dimensional two-disk hyperchaotic dynamical system, bifurcation analysis, circuit realisation and FPGA-based TRNG implementation, International Journal of Computer Applications in Technology, 62(1)(2019), 20–35, doi:10.1504/IJCAT.2020.103921.
[31] Margaris A, Adamopoulos M, Solving nonlinear algebraic systems using artificial neural networks, In Proceedings of the 10th International Conference on Engineering Applications of Artificial Neural Networks, (2007), 107–120.
[32] Patil S, Patil KR, Patil CR, Patil SS, Performance overview of an artificial intelligence in biomedics: a systematic approach, International Journal of Information Technology, 12(2020), 963–973, doi:10.1007/s41870-018-0243-8.
[33] K.C. Iarosz et al., Mathematical model of brain tumour with glia-neuron Interactions and chemotherapy treatment, Journal of Theoretical Biology,368(2015), 113121, doi:10.1016/j.jtbi.2015.01.006.
[34] S. Khajanchi, Stability Analysis of a Mathematical Model for Glioma-Immune Interaction under Optimal Therapy, International Journal of Nonlinear Sciences and Numerical Simulation, 20(3-4)(2019), 269-285, doi:10.1515/ijnsns-2017-0206.
[35] E. Vargees Kaviyan, T. Jayakumar, S. Sujitha, D. Maheskumar, Analytical and Numerical Solutions for Glial Cells Interactions between Chemo-Immunotherapy and Cancer Cells, OPSEARCH, doi:10.1007/s12597-024-00812-x.
[36] S.T.R. Pinho, F.S. Bacelar, R.F.S. Andrade, H.I. Freedman, A mathematical model for the effect of anti-angiogenic therapy in the treatment of cancer tumours by chemotherapy, Nonlinear Analysis: Real World Applications, 14(1)(2013), 815-828, doi:10.1016/j.nonrwa.2012.07.034. [37] J.S. Spratt,

T.L. Spratt, Rates of growth of pulmonary metastases and host survival, Annals of Surgery, 159(1964), 161-171, doi:10.1097/00000658-196402000-00001.
[38] W. Rzeski et al., Anticancer agents are potent neurotoxins in vitro and in vivo, Annals of Neurology, 56(3)(2004), 351-360, doi:10.1002/ana.20185.
[39] Stupp R et al., Effects of radiotherapy with concomitant and adjuvant temozolomide versus radiotherapy alone on survival in glioblastoma in a randomised phase III study: 5-year analysis of the EORTC-NCIC trial, The LANCET Oncology 10(2009), 459-466, doi:10.1016/S1470-2045(09)70025-7.19
[40] Rana Said et al., Cyclophosphamide Pharmacokinetics in Mice: A Comparison Between Retro Orbital Sampling Versus Serial Tail Vein Bleeding, The Open Pharmacology Journal, 1(2007), 30-35, doi:10.2174/1874143600701010030.
[41] Azevedo FAC et al., Equal numbers of neuronal and non-neuronal cells make the human brain an isometrically scaled up primate brain, Journal of Comparative Neurology, 513(5)(2009), 532-541, doi:10.1002/cne.21974.
[42] N. Kronik, Y. Kogan, V.Vainstein, Z. Agur, Improving alloreactive CTL immunotherapy for malignant gliomas using a simulation model of their interactive dynamics, Cancer immunology, immunotherapy, 57(3)2008, 425-439, doi:10.1007/s00262-0070387-z.
[43] H.H. Dubben, H.D. Thames, and H.P.B. Bornholdt, Tumor volume: a basic and specific response predictor in radiotherapy, Radiotherapy and Oncology, 47(2)(1998), 167-174, doi:10.1016/s0167-8140(97)00215-6.
[44] J. Vaage, Influence of tumour antigen on maintainance versus depression of tumour specific immunity, Cancer Research, 33(3)(1973), 493-503.
[45] Tian, Y.; Su, D.; Lauria, S.; Liu, X. Recent advances on loss functions in deep learning for computer vision, Neurocomputing, 497(2022), 129–158, doi:10.1016/j.neucom.2022.04.127. [46] Ul Rahman, J.; Ali, A.; Ur Rehman, M.; Kazmi, R. A unit softmax with Laplacian Smoothing stochastic gradient descent for deep convolutional neural networks. In Proceedings of the Intelligent Technologies and Applications: Second International Conference, INTAP 2019, Bahawalpur, Pakistan, 6–8 November 2019; Springer: Singapore, 2020, doi:10.1007/978-981-15-5232-8.
[47] Chen, F.; Sondak, D.; Protopapas, P.; Mattheakis, M.; Liu, S.; Agarwal, D.; Di Giovanni, M. Neurodiffeq: A python package for solving differential equations with neural networks, The Journal of Open Source Software, 5(46)(2020), 1931, doi:10.21105/joss.01931.
[48] Roy, S.K.; Manna, S.; Dubey, S.R.; Chaudhuri, B.B. LiSHT: Non-parametric linearly Scaled hyperbolic tangent activation function for neural networks. In International Conference on Computer Vision and Image Processing, Nagpur, India, 4–6 November 2022; Springer Nature: Cham, Switzerland, 2022, (2023), doi:10.1007/978-3-03131407-0 35.
[49] Qi, J.; Du, J.; Siniscalchi, S.M.; Ma, X.; Lee, C.-H. On mean absolute error for deep neural network based vector-to-vector regression. IEEE Signal Processing Letters 2020, 27, 1485–1489, doi:10.1109/LSP.2020.3016837. 20
[50] Wright, L.G.; Onodera, T.; Stein, M.M.; Wang, T.; Schachter, D.T.; Hu, Z.; McMaon, P.L.Deep physical neural networks trained with backpropagation. Nature, 601, 549–555, 2022, doi:10.1038/s41586-021-04223-6.